ACS APPLIED MATERIALS & INTERFACES

Research Article

www.acsami.org

Cysteamine-Based Cell-Permeable Zn^{2+}-Specific Molecular Bioimaging Materials: From Animal to Plant Cells

Sougata Sinha,[†] Gourab Dey,[†] Sunil Kumar,[†] Jomon Mathew,[‡] Trinetra Mukherjee,[§] Subhrakanti Mukherjee,*[,§] and Subrata Ghosh*[,†]

[†]School of Basic Sciences, Indian Institute of Technology Mandi, Mandi, H.P. 175001, India

[‡]Schulich Faculty of Chemistry and the Lise Meitner Minerva Center for Computational Quantum Chemistry, Technion-Israel Institute of Technology, Haifa 32000, Israel

[§]Department of Microbiology, Burdwan University, Burdwan, West Bengal 713101, India

Supporting Information

ABSTRACT: Structure-interaction/fluorescence relationship studies led to the development of a small chemical library of Zn^{2+}-specific cysteamine-based molecular probes. The probe **L5** with higher excitation/emission wavelengths, which absorbs in the visible region and emits in the green, was chosen as a model imaging material for biological studies. After successful imaging of intracellular zinc in four different kinds of cells including living organisms, plant, and animal cells, in vivo imaging potential of **L5** was evaluated using plant systems. In vivo imaging of translocation of zinc through the stem of a small herb with a transparent stem, *Peperomia pellucida*, confirmed the stability of **L5** inside biological systems and the suitability of **L5** for real-time analysis. Similarly, fluorescence imaging of zinc in gram sprouts revealed the efficacy of the probe in the detection and localization of zinc in cereal crops. This imaging technique will help in knowing the efficiency of various techniques used for zinc enrichment of cereal crops. Computational analyses were carried out to better understand the structure, the formation of probe–Zn^{2+} complexes, and the emission properties of these complexes.

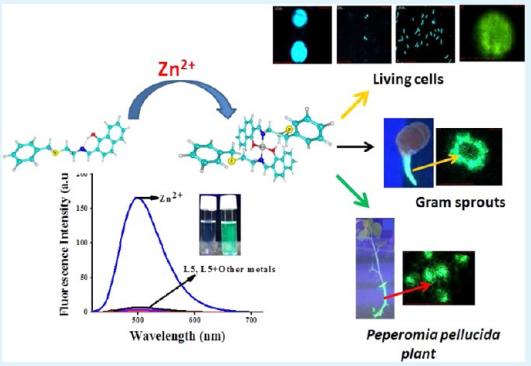

KEYWORDS: *molecular marker, fluorescence bioimaging, intracellular zinc, turn-on, live plant imaging*

INTRODUCTION

Metal-ion-induced fluorescence enhancement of small molecules has been the potential tool for the last few decades to obtain additional insight into various biological events including the distribution and concentration of these metal ions in living cells.[1−4] One of the major applications of this tool is metal ion sensing/imaging/labeling in living cells through rendering a strong fluorescent signal. For a molecular probe to be successful in fluorescence imaging of metal ions in living cells, the main criteria are its easy cell membrane permeation property, having a higher excitation/emission wavelength to reduce/stop damaging of cellular tissues, instantaneous interaction with the metal ion producing a bright fluorescence signal, and more importantly selective for a particular metal ion over all other metal ions present in the biological milieu.

Divalent zinc, Zn^{2+}, is one of the most diversely studied biologically important metals. Zinc has been found to be the second most abundant transition heavy metal ion in a normal human body, and it occupies the 24th position among the most abundant elements in Earth's crust.[5,6] Zinc is involved in a large number of biological processes which include neurotransmission,[7,8] enzyme regulation,[9] apoptosis,[10] gene expression,[11] etc. In addition to these, Zn^{2+} has been found to be critical for numerous cellular functions.[12] The concentration range of Zn^{2+} in different biological cells may vary from 1 nM to about 1 mM.[13,14] However, because of its closed-shell $3d^{10}4s^0$ electronic configuration Zn^{2+} shows neither any type of magnetic signals nor the convenient spectroscopic signature. Therefore, imaging of labile or free intracellular Zn^{2+} using a fluorescence microscopy technique is an important area of research for studying various intracellular events, which involve Zn^{2+}, including the role of Zn^{2+} in the regulation of cell growth. Often organic molecular probes are used as efficient chemical devices to image intracellular zinc.[4,6,15−53] The molecular probes which have a strong fluorescence property often suffer from a background fluorescence problem. Though many fluorescence and fluorogenic sensors based on small molecules for imaging of zinc in living systems have been developed in the last few years, and despite their strong potential in bioimaging of zinc, some of them suffer from drawbacks such as lengthy synthesis procedures that are followed for their preparation that limit their easy availability, background fluorescence problem,

Received: August 16, 2013
Accepted: November 1, 2013
Published: November 1, 2013

 © 2013 American Chemical Society

Scheme 1. Syntheses of L1−L7

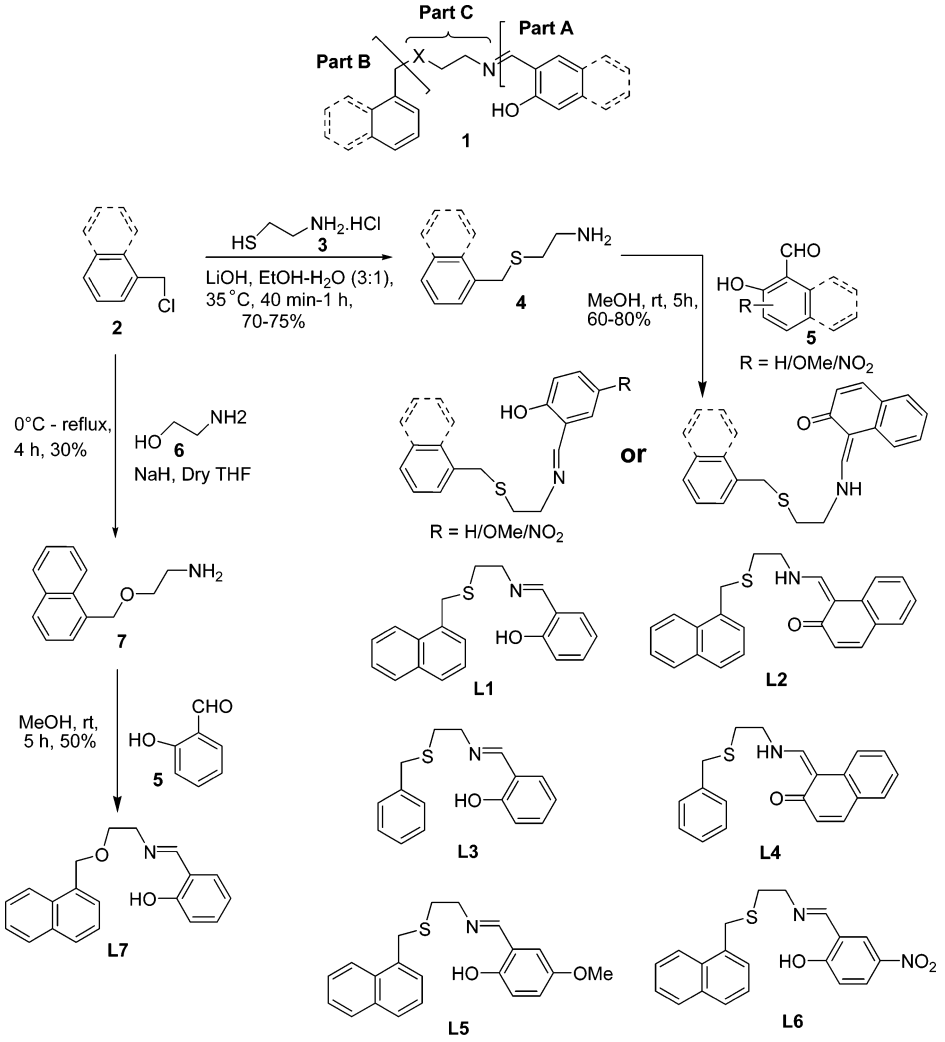

and affinity towards the biorelevant competitors $Na^+/K^+/Ca^{2+}/Mg^{2+}$. In addition to these, easy and inexpensive methods for checking the biostability and real-time analysis potential of newly developed molecular probes are rarely reported. Therefore, this is an ongoing endeavour to develop an easy synthesizable novel small-molecule-based non-/weak-fluorescent cell-permeable molecular probe which upon interaction with Zn^{2+} results in a strong fluorescent signaling with considerably high fluorescence quantum yield.

Cysteamine is a naturally occurring aminothiol and is used widely as an important building block for many natural products.[54,55] In addition to its biological importance as an essential part of Coenzyme A, cysteamine is equally important as therapeutic for the treatment of nephropathic cystinoss.[56,57] In most of the cases, the thiol terminal of cysteamine is protected by an aryl functionality resulting in the formation of β-arylmercaptoethyl amine as an intermediate containing a reactive amine terminal. Whenever needed, the aryl protection is removed to retrieve the thiol functionality.[54,55] These β-arylmercaptoethyl amines have found wide applications in synthesizing wide-ranging small molecules and liagnds that are ultimately used either in biological or in diagnostic studies.[54] On the other hand, many salen-based derivatives have been found to have strong affinity towards Zn^{2+} and render turn-on fluorescence signaling upon interaction with Zn^{2+}. As the β-arylmercaptoethyl amine-based many small molecules have shown considerable biostability and biocompatibility,[54,58] we became curious to explore the reactivity of the amine terminal towards the formation of salen derivatives and to investigate the potential of these newly developed probes in bioimaging of zinc.

Herein, we report our recent studies on systematic development of cysteamine-based novel Zn^{2+}-specific cell-permeable molecular markers for fluorescence imaging of zinc in living system, both in vitro and in vivo. Structure-interaction/fluorescence relationship studies enabled us to develop a potent probe which absorbs in the visible region and emits in the green. Four different cells, starting from animal to plant cells, have been used to reconfirm the probe's efficiency. In vivo imaging potential was proved using plant systems.

EXPERIMENTAL SECTION

Materials. Solvents and chemicals were purchased from commercial sources and used as received. Spectroscopic grade solvents were used for spectral measurements. Nitrate salts of Li^+, Na^+, K^+, Ca^{2+}, Mg^{2+}, Fe^{3+}, Cu^{2+}, Zn^{2+}, Cd^{2+}, Co^{2+}, Sr^{2+}, Pb^{2+}, Ba^{2+}, and Ni^{2+} and chloride salts of Mn^{2+} and Hg^{2+} were used for spectroscopic studies. Tetrabutyl ammonium salts of Cl^-, Br^-, I^-, F^-, CH_3COO^-, NO_3^-, ClO_4^-, and CN^- were used for investigating anion effects. Metal salts were dissolved in Milli-Q water at pH 7.0. Anions were dissolved in DMF.

Instruments. ^{1}H and ^{13}C NMR spectra were recorded on Jeol JNM ECX 400 MHz and Bruker Avance 300 MHz spectrometers in $CDCl_3$ and DMSO-d_6. UV−vis and fluorescence spectra were recorded on Shimadzu UV-2450 and Cary Eclipse fluorescence spectrophotometer, respectively. FT-IR spectra were recorded on a Perkin Elmer Spectrum 2 spectrophotometer. LSMS-ESI and HRMS-ESI spectra were recorded on a Q-TOF micromass and WATERS-Q-Tof Premier spectrometer, respectively. The imaging system was comprised of an inverted fluorescence microscope (Leica DM 1000 LED), a digital compact camera (Leica DFC 420C), and an image processor (Leica Application Suite v3.3.0). The microscope was equipped with a mercury 50 W lamp.

Syntheses of Probes. The synthesis procedures that were followed to synthesize the molecular probes of interest for this study are outlined in Scheme 1. A condensation reaction between cysteamine hydrochloride (**3**) and aryl chlorides (**2**) yielded *β*-arylmercaptoethyl amines (**4**).[55] Next, the amines **4** were reacted with the respective aldehydes (**5**) to obtain the desired probes **L1**−**L6**. To replace the thioether functionality of **L1** by the oxa-ether one, aryl halide (**4**) was converted first to the intermediate **6**,[59] which upon reaction with aldehyde **5** resulted in the formation of probe **L7**. All the intermediates and final products were characterized using spectroscopic techniques such as FT-IR, NMR, and mass spectroscopy (Supporting Information).

All *β*-arylmercaptoethylamines were synthesized following a literature reported procedure,[55] and the products were obtained in good yields. *β*-Naphthaylmethoxyethylamine was synthesized following another reported procedure.[59] For known compounds, viz., *β*-benzylmercaptoethylamine and *β*-naphthaylmethoxyethylamine, the spectroscopy data were in agreement with the reported data.

***β*-Naphthaylmercaptoethylamine.** Yield: 70%; Light yellow viscous liquid; ^{1}H-NMR (300 MHz, $CDCl_3$-DMSO) δ 2.54 (t, J = 6.6, 2H), 2.77 (t, J = 6.4, 2H), 4.18 (s, 2H), 7.40−7.42 (m, 2H), 7.49−7.55 (m, 2H), 7.78−7.80 (m, 1H), 7.87−7.89 (m, 1H), 8.13−8.18 (m, 1H); ^{13}C-NMR (100 MHz, DMSO) δ 38.9, 39.1, 40.1, 124.4, 125.3, 125.8, 125.9, 127.1, 127.7, 128.6, 130.9, 133.7, 134.2; MS (TOF-ES) m/z calculated for $C_{13}H_{16}NS$ $[MH]^+$ 218.10, found 218.36.

General Procedure for the Synthesis of Schiff Bases L1−L7. Amines (5 mmol) were dissolved in methanol followed by dropwise addition of various salicylaldehydes (5 mmol) to the same solution. The whole mixture was kept stirring for 4−5 h at room temperature. In the case of solid product, the precipitate was filtered, washed with methanol, and dried under vacuo. The liquid products were purified by column chromatography using a mixture of ethyl acetate and hexane as eluent.

*2-((2-((Naphthalen-4-yl)methylthio)ethylimino)methyl)phenol (**L1**).* Yield: 70%; Light yellow solid; Melting point 62−63 °C; FT-IR (KBr, ν in cm^{-1}) 639, 755, 783, 800, 894, 983, 1044, 1206, 1278, 1333, 1394, 1417, 1444, 1466, 1506, 1583, 1633, 2856, 2933, 3011, 3044; ^{1}H-NMR (300 MHz, $CDCl_3$) δ 2.81 (t, J = 6.4 Hz, 2H), 3.76 (t, J = 6.4 Hz, 2H), 4.27 (s, 2H), 6.86−6.93 (m, 2H), 7.33−7.54 (m, 6H), 7.84 (d, J = 7.7 Hz, 1H), 7.92−7.95 (m, 1H), 8.13−8.17 (m, 1H), 8.47 (s, 1H), 13.40 (s, 1H); ^{13}C-NMR (75 MHz, $CDCl_3$) δ 33.2, 35.1, 59.6, 117.5, 119.0, 124.5, 125.6, 126.4, 126.6, 127.6, 128.7, 129.3, 131.7, 131.8, 132.8, 134.0, 134.5, 161.5, 166.4; HRMS m/z calculated for $C_{20}H_{20}NOS$ $[MH]^+$ 322.1265, found 322.1264.

*(1Z)-1-((2-((Naphthalen-4-yl)methylthio)ethylamino)methylene)-naphthalen-2(1H)-one (**L2**).* Yield: 70%; Yellow solid; Melting point 88−91 °C; FT-IR (KBr, ν in cm^{-1}) 739, 772, 833, 917, 989, 1017, 1133, 1178, 1206, 1283, 1361, 1400, 1450, 1494, 1550, 1633, 2933, 3061; ^{1}H-NMR (300 MHz, $CDCl_3$) δ 2.81 (t, J = 6.4 Hz, 2H), 3.53 (t, J = 6.1 Hz, 2H), 4.22 (s, 2H), 6.95−6.99 (m, 1H), 7.26−7.31 (m, 1H), 7.38−7.54 (m, 4H), 7.64 (d, J = 7.6 Hz, 1H), 7.69−7.74 (m, 2H), 7.80−7.83 (m, 1H), 7.88−7.91 (m, 1H), 8.12−8.15 (m, 1H), 8.51 (s, 1H), 14.49 (s, 1H); ^{13}C-NMR (75 MHz, $CDCl_3$) δ 33.3, 35.3, 53.9, 107.2, 118.6, 123.2, 124.4, 124.8, 125.6, 126.4, 126.7, 127.7, 128.3, 128.9, 129.3, 129.6, 131.6, 133.8, 134.0, 134.5, 137.5, 159.2, 175.4; HRMS m/z calculated for $C_{24}H_{22}NOS$ $[MH]^+$ 372.1422, found 372.1421.

*2-((2-(Benzylthio)ethylimino)methyl)phenol (**L3**).*[60] Yield: 60%; Yellow viscous liquid (as obtained); FT-IR (Neat, ν in cm^{-1}) 706, 757, 1154, 1282, 1416, 1450, 1495, 1579, 1635, 2842, 2921, 3033, 3061; ^{1}H-NMR (300 MHz, $CDCl_3$) δ 2.77 (t, J = 6.7 Hz, 2H), 3.70−3.76 (m, 4H), 6.88−7.00 (m, 2H), 7.26−7.34 (m, 7H), 8.29 (s, 1H), 13.3 (s, 1H); ^{13}C-NMR (100 MHz, $CDCl_3$) δ 32.1, 36.6, 59.1, 117.0, 118.6, 127.1, 128.6, 128.9, 129.05, 131.4, 132.3, 138.2; HRMS m/z calculated for $C_{16}H_{18}NOS$ $[MH]^+$ 272.1109, found 272.1102.

*(1Z)-1-((2-(Benzylthio)ethylamino)methylene)naphthalen-2(1H)-one (**L4**).* Yield: 75%; Yellow solid; Melting point 69−71°C; FT-IR (KBr, ν in cm^{-1}) 694, 761, 839, 889, 1011, 1144, 1189, 1283, 1317, 1361, 1439, 1500, 1539, 1628, 2917, 2933, 3028; ^{1}H-NMR (300 MHz, $CDCl_3$) δ 2.76 (t, J = 6.6 Hz, 2H), 3.65 (t, J = 6.6 Hz, 2H), 3.76 (s, 2H), 6.97 (d, J = 9.2 Hz, 1H), 7.25−7.35 (m, 6H), 7.45−7.5 (m, 1H), 7.64−7.73 (dd, J = 9.2 Hz, 13.6 Hz, 2H), 7.88 (d, J = 8.3 Hz, 1H), 8.67 (s, 1H), 14.5 (s, 1H); ^{13}C-NMR (75 MHz, $CDCl_3$) δ 32.6, 37.1, 53.8, 107.3, 118.5, 123.3, 124.8, 126.8, 127.7, 128.4, 129.1, 129.4, 129.7, 134.1, 137.5, 138.4, 159.1, 175.4; HRMS m/z calculated for $C_{20}H_{20}NOS$ $[MH]^+$ 322.1265, found 322.1264.

*2-((2-((Naphthalen-4-yl)methylthio)ethylimino)methyl)-4-methoxyphenol (**L5**).* Yield: 70%; Yellow semi solid; FT-IR (Neat, ν in cm^{-1}) 783, 1033, 1156, 1228, 1267, 1333, 1394, 1461, 1499, 1589, 1633, 2844, 2917, 3061; ^{1}H-NMR (300 MHz, $CDCl_3$) δ 2.84 (t, J = 6.7 Hz, 2H), 3.65 (t, J = 6.6 Hz, 2H), 3.81(s, 3H), 4.21 (s, 2H), 6.71 (s, 1H), 6.92−6.97 (m, 2H), 7.39−7.42 (m, 2H), 7.51−7.57 (m, 2H), 7.78−7.90 (m, 2H), 8.10−8.16 (m, 2H), 12.77 (s, 1H); ^{13}C-NMR (100 MHz, $CDCl_3$) δ 32.9, 34.8, 56.0, 59.4, 114.9, 117.8, 118.3, 119.4, 124.2, 125.2, 125.9, 126.2, 127.2, 128.4, 128.9, 131.4, 133.7, 134.2, 152.0, 155.3, 165.8; HRMS m/z calculated for $C_{21}H_{22}NO_2S$ $[MH]^+$ 352.1371, found 352.1371.

*2-((E)-(2-((Naphthalen-4-yl)methylthio)ethylimino)methyl)-4-nitrophenol (**L6**).* Yield: 80%; Yellow solid; Melting point 134−135°C; FT-IR (KBr, ν in cm^{-1}) 672, 722, 772, 839, 894, 927, 961, 1017, 1044, 1100, 1161, 1189, 1239, 1278, 1400, 1439, 1533, 1556, 1650, 1928, 2411; ^{1}H-NMR (300 MHz, $CDCl_3$) δ 2.87 (t, J = 5.7 Hz, 2H), 3.50 (t, J = 5.8 Hz, 2H), 4.20 (s, 2H), 6.93 (d, J = 9.2 Hz, 1H), 7.40−7.44 (m, 2H), 7.57−7.58 (m, 2H), 7.71 (s, 1H), 7.82 (d, J = 7.0 Hz, 1H), 7.90 (s, 1H), 7.99 (s, 1H), 8.13−8.19 (m, 2H), 14.5 (s, 1H); ^{13}C-NMR (75 MHz, $CDCl_3$) δ 33.2, 35.6, 57.5, 117.0, 119.6, 124.6, 125.7, 126.8, 126.9, 127.6, 128.8, 129.0, 129.1, 131.7, 134.1, 134.7, 139.3, 165.8, 169.8; HRMS m/z calculated for $C_{20}H_{19}N_2O_3S$ $[MH]^+$ 367.1116, found 367.1116.

*2-((2-((Naphthalen-4-yl)methoxy)ethylimino)methyl)phenol (**L7**).* Yield: 50%; Yellow viscous liquid (as obtained); FT-IR (Neat, ν in cm^{-1}) 757, 790, 1098, 1277, 1461, 1489, 1579, 1629, 2859, 2921, 3049; ^{1}H-NMR (400 MHz, $CDCl_3$) δ 3.77−3.79 (m, 2H), 3.83−3.86 (m, 2H), 4.97 (s, 2H), 6.84−6.87 (m, 1H), 6.97 (d, J = 8.3 Hz, 1H), 7.15−7.2 (dd, J = 7.4 Hz, 9.08 Hz, 1H), 7.25 (s, 1H), 7.29−7.33 (m, 2H), 7.39−7.46 (m, 3H), 7.79−7.83 (m, 1H), 8.02 (d, J = 8.4 Hz, 1H), 8.30 (s, 1H), 11.4 (s, 1H); ^{13}C-NMR (100 MHz, $CDCl_3$) δ 59.1, 69.5, 72.0, 118.4, 124.1, 125.1, 126.2, 126.5, 128.4, 128.7, 131.4, 132.2, 161.2, 166.5; HRMS m/z calculated for $C_{20}H_{20}NO_2$ $[MH]^+$ 306.1494, found 306.1497.

Spectroscopic Measurements. Different amounts of concentrated analyte solutions were added to a 3 mL ligand solution to avoid dilution error. For the titration of in situ generated complexes, 3 mL of ligand solutions was taken in a cuvette, and 20 μM Zn^{2+} was added to it. UV−vis and fluorescence spectroscopic measurements were done immediately after addition of the various analytes. For fluorescence measurements, the excitation wavelength was fixed at 370 nm (λ_{ex} = 370 nm) for **L1**, **L3**, **L6**, and **L7** and at 383 nm (λ_{ex} = 383 nm) for **L2** and **L4**. The excitation wavelength for **L5** was fixed at 400 nm. A 1 cm quartz cell with a slit width of 5 nm for both excitation and emission was used throughout the fluorescence measurements. All the spectroscopic measurements were performed at 25 °C. Fluorescence quantum yields were calculated using quinine sulfate as standard reference.

Binding Constant Calculation Using Fluorescence Titration. The equation used[61,62]for binding constant calculation, based on 2:1 stoichiometry, is $[G]_{tot} = a/2K_{21}(1 - a)^2[H]_{tot} + a[H]_{tot}/2$, where

$[G]_{tot}$ is total concentration of guest (here Zn^{2+}); $[H]_{tot}$ is the total concentration of host; $a = (I - I_o)/(I_{inf} - I_o)$ where I is the fluorescent intensity at a particular Zn^{2+} concentration; and I_o and I_{inf} are the intensities at zero and infinite Zn^{2+} concentrations, respectively. From the fluorescence titration $(I - I_o)/(I_{inf} - I_o)$ is plotted against $[Zn^{2+}]_{tot}$.

Cell Culture and Intracellular Zinc Imaging (In Vitro Studies). *Candida albicans* (Imtech No. 3018) and *Bacillus thuringiensis* (strain isolated in our laboratory as a biopesticide agent for controlling looper pest of tea and identified on the basis of 16S rDNA gene sequence homology) cells from exponentially growing culture in potato dextrose broth (pH 5.2, incubation temperature 37 °C) and nutrient broth (pH 7.2, incubation temperature 29 °C), respectively, were collected by centrifugation at 3000 rpm for 5 min. Pollen grains were obtained from freshly collected mature buds of *Tecoma stans*, a common ornamental plant of the Bignoniaceae family. After crushing the stamens on a sterile Petri plate and suspending them in 0.1 M HEPES buffer (pH 7.4), debris were removed by filtering through a thin layer of nonabsorbent cotton. Suspended pollens were subjected to centrifugation at 3000 rpm for 5 min. All three types of cells were washed twice by suspending them in 0.1 M HEPES buffer (pH 7.4) followed by centrifugation in the same speed as above. Then washed cells were treated separately with $Zn(NO_3)_2 \cdot 6H_2O$ (50 μM) for 30 min. After incubation, the cells were again washed with 0.1 M HEPES buffer (pH 7.4) and then incubated with 50 μM **L5** for another 30 min. Treated cells were washed further to reduce background fluorescence. For animal cells, the fish eggs were collected from *Puntius sarana sarana* and washed thoroughly with normal saline to remove unwanted tissues and to make the eggs separate from each other. The separated eggs were then treated with Zn^{2+} (50 μM) for 30 min followed by **L5** (50 μM) for another 30 min. Finally, the cells were mounted on grease-free glass slides and observed under a Leica DM 1000 Fluorescence microscope with UV filter. Cells treated with Zn^{2+} but not with ligand and cells without Zn^{2+} treatment but incubated with ligand were used as control. All imaging experiments were done in phosphate-free buffer.

Tnaslocation of Zn^{2+} in a Whole-Plant (In Vivo Studies). For tracking translocation of zinc through stem using **L5** in *Peperomia pellucida* (family Piperomiacea), a small herbaceous plant with transparent stem was used. Freshly collected plants were thoroughly washed to remove soil and dirt, and then the roots of the plant were dipped into Zn^{2+} solution (5×10^{-4} M). One hour later, the dipped portion of the root was washed several times to remove externally bound zinc ion, if any, and again the root was dipped into a solution of **L5** (5×10^{-4} M). The tube containing **L5** solution was covered with black paper, but the top portion of the tube was kept open in such a way that the top portion of the plant got sunlight exposure to ensure transpirational loss of water resulting in efficient sucking of Zn^{2+} through the root.

Imaging of Zinc in Gram Sprouts (In Vivo Studies). Matured gram seeds were germinated at room temperature using distilled water. After treating with Zn^{2+} (5×10^{-4} M) solution for two hours the sprouted seeds were washed several times with water to remove surface sticking Zn^{2+}. Next, a few of the incubated seeds were further incubated with probe **L5** (5×10^{-4} M) for one hour and washed several times before sectioning. Finally, the sections were imaged using a fluorescence microscope. Sprout sections treated with Zn^{2+} but not with ligand **L5** and sections without Zn^{2+} treatment but incubated with probe **L5** were used as control.

RESULT AND DISCUSSION

UV–Vis and Fluorescence Studies. At the very outset of these studies only **L1** and **L2** were synthesized (Scheme 1), and their photophysical properties, in the presence and absence of various metal ions, were thoroughly studied. The probe **L1** (10 μM) showed absorption peaks at 288 nm ($\varepsilon = 0.121 \times 10^5$), 299 nm ($\varepsilon = 0.101 \times 10^5$), and 318 nm ($\varepsilon = 0.057 \times 10^5$) due to n–p* and p–p* transitions in DMF. Addition of 20 μM Zn^{2+} into the solution of **L1** resulted in a new band centered at 370 nm with the disappearance of a peak at 318 nm. In addition, an increase in the absorption maxima of peaks at 298 and 285 nm (as compared to **L1**) was observed. Very little blue shift was observed in the case of the 288 nm band. The isosbestic point at 334 nm clearly indicated complexation between **L1** and Zn^{2+} (Figure S1, Supporting Information). Generation of a new band at higher wavelength (370 nm) was due to internal charge transfer (ICT).[63]

Due to *E*/*Z*-isomerization and excited state proton transfer (ESPT), **L1** was found to be weak fluorescent. The addition of aqueous Zn^{2+} to **L1** solution induced strong blue fluorescence at 448 nm (λ_{em}) when excited at 370 nm (λ_{ex}) (Figure 1 and

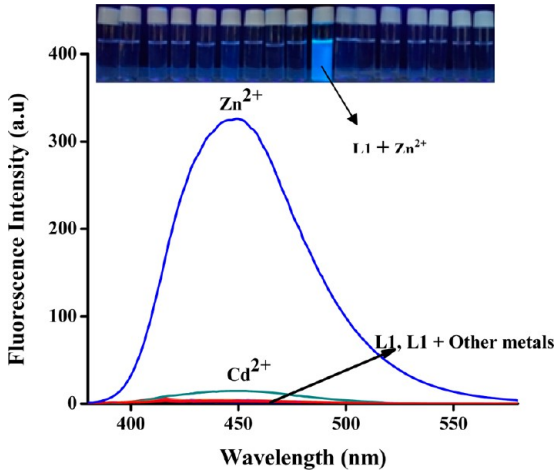

Figure 1. Emission spectra of **L1** (10 μM) in DMF in the presence of 20 μM biologically and environmentally important metals (Li^+, Na^+, K^+, Ca^{2+}, Mg^{2+}, Fe^{3+}, Cu^{2+}, Zn^{2+}, Cd^{2+}, Co^{2+}, Sr^{2+}, Pb^{2+}, Ba^{2+}, Ni^{2+}, Mn^{2+}, Hg^{2+}) in filtered Milli-Q water. Top: Color change of **L1** (10 μM) after addition of Zn^{2+} (20 μM) and other metals (100 μM) under a 365 nm UV lamp.

Figures S2 and S3, Supporting Information). No such significant effect on the emission spectra of **L1** was observed upon the addition of an excess amount of a large number of other different metals (Figure S4, Supporting Information). Often, the molecular probes which show turn-on fluorescence signaling upon interaction with Zn^{2+} also interact with Cd^{2+}/Pb^{2+} and result in a turn-on signaling. **L1** did not show any significant fluorescence enhancement in the presence of Cd^{2+}/Pb^{2+}. This fluorescence enhancement can be ascribed mainly to the ICT mechanism.[63,64] While binding of zinc with **L1** suppressed *E*/*Z*-isomerization and also ruled out the scope of the ESPT mechanism, zinc coordination to the hydroxyl group induced an effective ICT effect in part A resulting in an enhancement in fluorescence. That ICT played an important role in fluorescence enhancement was supported further by the fluorescence enhancement in the presence of highly basic anions, viz., acetate and fluoride (Figures S5a and S6, Supporting Information), while most of the other common anions (Cl^-, Br^-, I^-, NO_3^-, ClO_4^-, CN^-) (Figure S7, Supporting Information) had very little effect on the emission spectra of **L1**–Zn^{2+}. ^1H NMR spectra clearly indicated downfield chemical shift of the imine proton of **L1** and almost disappearance of a signal for the phenolic proton in the presence of Zn^{2+} due to strong coordination of Zn^{2+} with imine nitrogen and phenolic oxygen (Figure S8, Supporting Information). As complete deprotonation of the phenolic proton occurred in the presence of acetate/fluoride, the

phenolate form of **L1** interacted with Zn^{2+} more strongly than the pure **L1** resulting in further fluorescence enhancement. This indicated that the ICT effect was more prominent in the presence of acetate/fluoride. The quantum yield of **L1**−Zn^{2+} was found to be 0.33 (a 0.5 M H_2SO_4 solution of quinine sulfate was used as standard). The generation of fluorescence turn-on signal immediately after the addition of Zn^{2+} to **L1** solution indicated instantaneous Zn^{2+}-sensing capability of **L1**. The fluorescence of the **L1**−Zn^{2+} ensemble was found to be stable for a minimum of 3 h (Figure S9, Supporting Information) indicating the possibility of using this probe for real-time analysis. A detection limit was calculated according to a literature method[65] and was found to be 1.41 μM (Figure S10, Supporting Information).

Stoichiometry of Metal Complexes. Job's method[66] suggested a 2:1 complexation ratio between **L1** and Zn^{2+} (Figure S11, Supporting Information), and the same was supported further by ESI mass spectra (Figure S12, Supporting Information). In mass spectra a peak at 706.16 (calculated 706.17) was observed which corresponds to $[2\mathbf{L1} + Zn]^+$. The binding constant was calculated using the Levenberg−Marquardt algorithm which showed high binding constant value 3.95×10^{11} M^{-2} for the **L1**−Zn^{2+} complex (Figure S13, Supporting Information).[61,62]

Structure-Interaction/Fluorescence Relationship Study. Though **L2**, like **L1**, was found to be weak fluorescent (10 μM, in DMF), very little fluorescence enhancement was observed upon the addition of Zn^{2+} (Figure S15, Supporting Information). A careful look at the NMR spectra revealed that, unlike **L1**, **L2** exists in keto form. In ^{13}C NMR, a peak at 175.4 corresponds to keto functionality (Figure S65, Supporting Information). The same has been observed in theoretical studies (see later sections for detail). Therefore the chemical structure of the binding sites played a major role in determining the affinity of the respective probe towards Zn^{2+}. One drawback of **L1** is its comparatively short excitation/emission wavelengths (λ_{ex} = 370 nm, λ_{em} = 448 nm). All these results made us curious to perform structure-interaction/fluorescence relationship studies to know about the structural influence of these probes towards their Zn^{2+} affinity and to develop probes with better excitation/emission wavelengths. To examine this, the basic structure **1** was parsed into three regions, viz., part A, part B, and part C, and we then systematically modified each region using our synthetic approach as described in Scheme 1. It is very clear from the previous discussion that part A, the one which is responsible for Zn^{2+} binding, plays an important role in determining the affinity/sensitivity of the probe towards Zn^{2+}. Whereas **L1**, **L3**, **L5**, and **L6** were synthesized by the reaction between β-arylmercaptoethyl amine and various salicylaldehydes, **L2** and **L4** were obtained from the condensation between β-arylmercaptoethyl amine and 2-hydroxy-1-naphthaldehyde. Both **L2** and **L4** preferred keto-form over enol-form. In **L7**, thio-ether functionality was replaced by oxa-ether functionality (part C).

Next, photophysical properties and binding affinity of these molecular probes towards Zn^{2+} were investigated carefully. All these ligands were found to be nonfluorescent. Like **L2**, **L4** showed very poor affinity towards Zn^{2+} (Figure S17, Supporting Information). Therefore, the keto-form of a probe bearing a basic structure of **1** becomes inactive towards Zn^{2+} binding. This was supported by **L6** which contains a strong electron-withdrawing group (NO_2) at the *para*-position of the OH group. Theoretical studies predict the keto form of **L6** is slightly more stable than the enol form (0.21 kcal/mol), and the activation barrier for the conversion of enol to keto form is only 2.84 kcal/mol. This suggests that there must be a delicate balance between the keto and enol form which can be easily altered by environmental effects. The first excited state (S1) geometry of both keto and enol form of **L6** is optimized at the CIS/6-311G(d,p)[67] level of theory, and the S1 state of the keto form is found to be 1.39 kcal/mol more stable than the S1 state of the enol form. Though NMR spectra indicated that the enol form is slightly more stable in the ground state (Figure S73, Supporting Information), it is quite logical that in the excited state **L6** adapts predominantly the keto-form due to easy activation of the ESPT mechanism (as an activation barrier between the keto and enol forms is very small). As fluorescence is an excited state phenomenon, **L6** did not interact with Zn^{2+} in the excited state resulting in no change in fluorescence property (Figure S19, Supporting Information). For **L3**−/**L7**−Zn^{2+} ensembles, the excitation/emission wavelengths were similar to the **L1**−Zn^{2+} ensemble (Figures S21 and S28, Supporting Information). In addition, **L3** showed some extent of fluorescence enhancement in the presence of other metal ions (Figure S24, Supporting Information) which are found often in cellular environment. However, the interesting outcome of this whole structure-fluorescence/interaction relationship study was the development of probe **L5**. The introduction of strong electron-donating functionality (OCH_3) at the *para*-position of OH changed the excitation/emission wavelengths (λ_{ex} = 400 nm and λ_{em} = 498 nm) of **L5** to a greater extent as compared to **L1**, **L3**, and **L7** (Supporting Information, Table 1). The **L5**−Zn^{2+} ensemble showed an absorption band (376−450 nm) in the visible region (Figure S34, Supporting Information) and an emission band (421−700 nm) in the green region (Figure 2). The requirement of higher

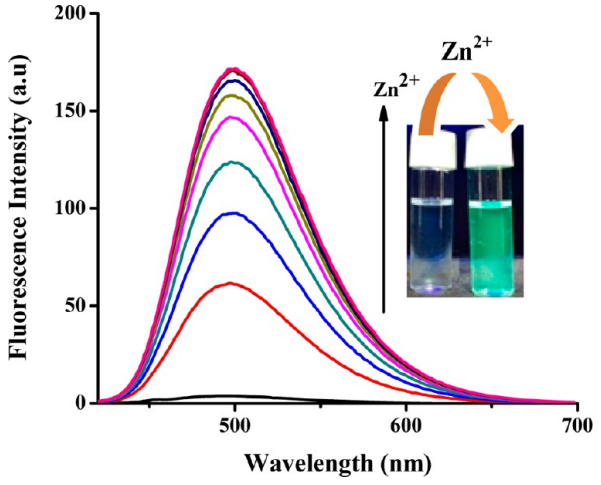

Figure 2. Emission spectrum of **L5** (10 μM) in DMF in the presence of increasing concentration of Zn^{2+} (0−20 μM) in filtered Milli-Q water.

equivalents of zinc for obtaining maximum fluorescence emission is due the existence of a fast equilibrium between free and solvated zinc making only part of the added zinc accessible to probe **L5** to render fluorescence signalling. In addition to the changes in excitation and emission wavelengths, **L5** did not show any fluorescence enhancements when treated with a large number of other metal ions including biologically important metal ions (Figure S37, Supporting Information).

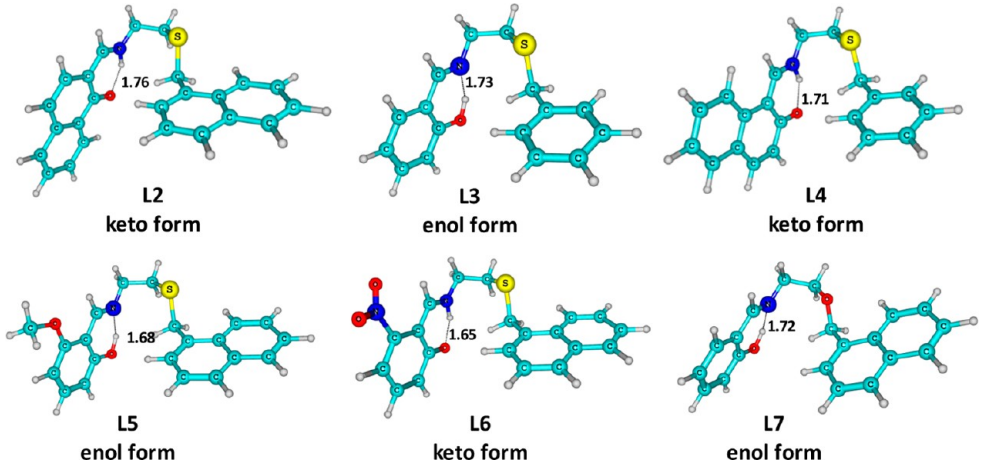

Figure 3. Optimized structure of ligands **L2**–**L7**.

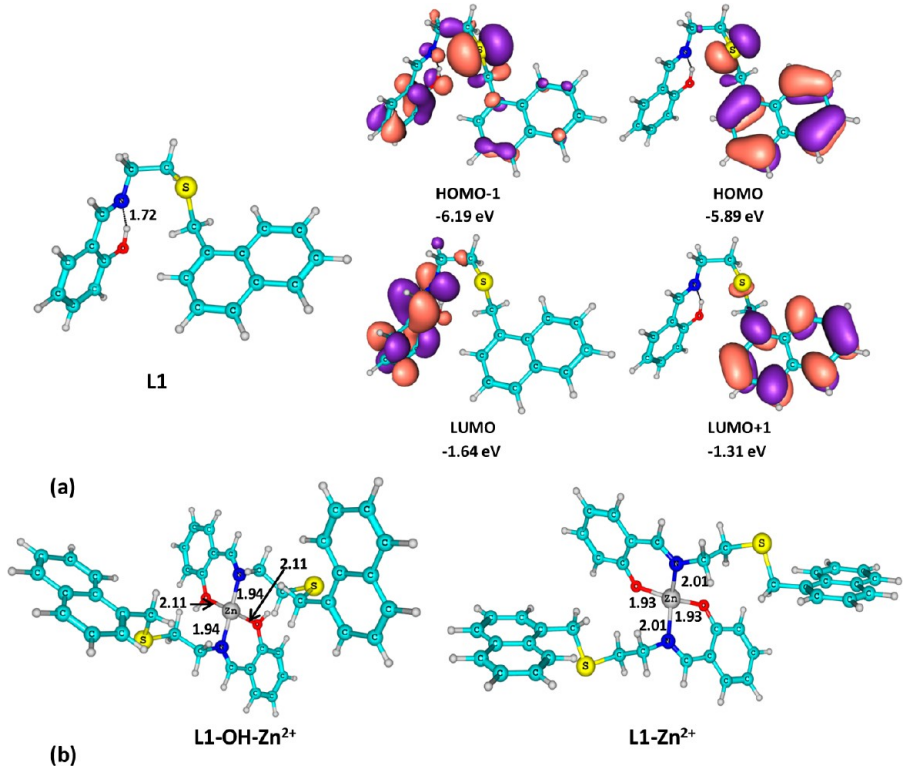

Figure 4. (a) Optimized structure of **L1** and the frontier molecular orbitals (isocontour at 0.03 au). (b) Optimized structure of **L1**–**OH**–Zn^{2+} and **L1**–Zn^{2+}.

Thus, **L5** can be considered as a Zn^{2+}-specific turn-on molecular probe. While checking the selectivity of the probe **L5** towards Zn^{2+}, the turn-on fluorescence response was observed in the presence of zinc competitors including its most biorelevant competitors $Na^+/K^+/Ca^{2+}/Mg^{2+}$ (Figure S38, Supporting Information). The limit of detection was found to be 1.31 μM, and the binding constant was 5.82×10^{10} M^{-2} (Figures S41 and S42, Supporting Information). Because of its better excitation/emission wavelengths, **L5** was chosen as a model compound for biological studies, both in vitro and in vivo. We also investigated the pH dependence of fluorescence emission of the **L5**–Zn^{2+} ensemble and observed the ensemble had stable fluorescence from pH 7.4 to 9 which is very much within the physiological range (Figures S43 and S44, Supporting Information).

Theoretical Study. Computational analyses have been carried out to better understand the structure, formation of Zn^{2+} complexes, and the emission properties of Zn^{2+} complexes. All calculations were carried out at the B3LYP/6-311G(d,p) level of density functional theory[68,69] using the Gaussian 09 suite of programs.[70] Since the formation of the keto-form is also possible for all ligands[71] and the stability of both the keto- and enol-forms can be influenced by the solvent, the keto- and enol-forms of all ligands were optimized in solvent phase using DMF as solvent employing the polarizable continuum model (PCM) (Figure 3)[72,73] implemented in Gaussian 09. It was found that the keto-form is more stable than the enol-form for ligands **L2**, **L4**, and **L6** by 2.93, 1.93, and 0.21 kcal/mol, respectively, while the remaining ligands prefer enol-form. The binding of Zn^{2+} to the keto-form of ligands

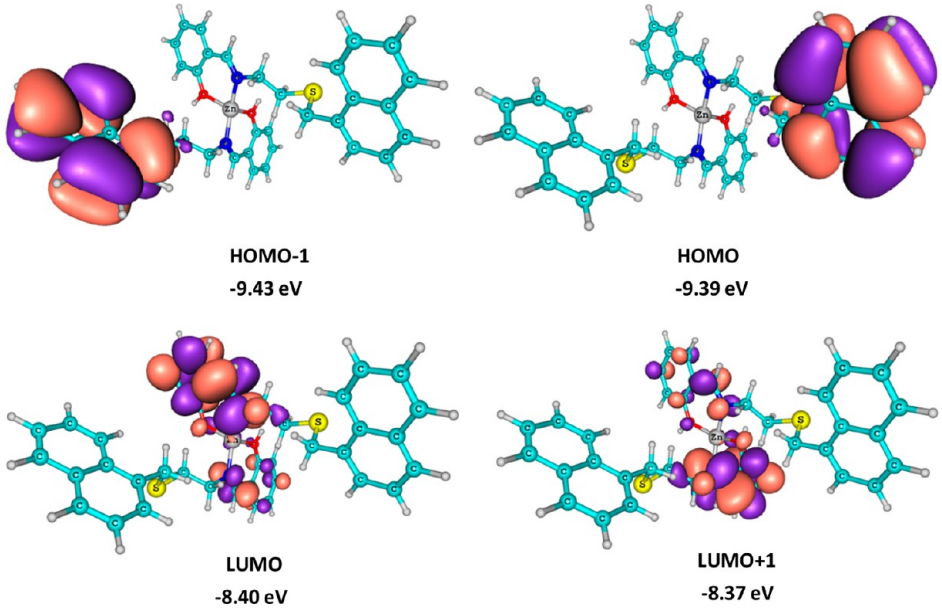

Figure 5. Frontier molecular orbitals of **L1−OH−Zn**$^{2+}$ (isocontour at 0.03 au).

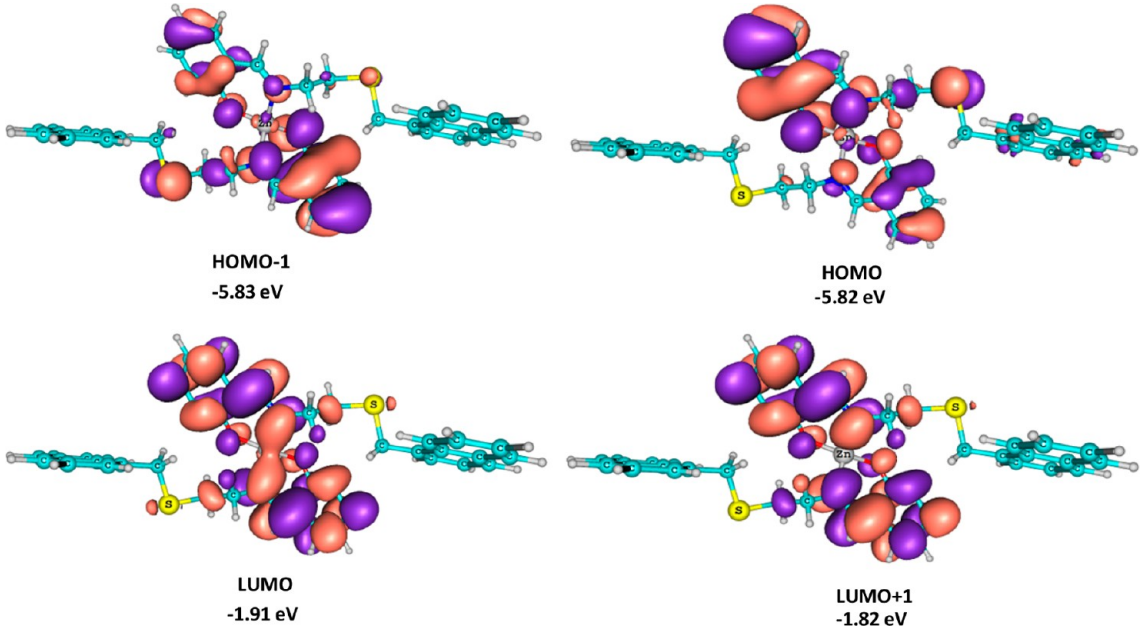

Figure 6. Frontier molecular orbitals of **L1−Zn**$^{2+}$ (isocontour at 0.03 au).

through O and N to form a chelate complex will be very ineffective compared to the enol-form since the N is more protected and the lone pair on N is not easily accessible. Further, NH hydrogen is less acidic than OH hydrogen. Such an ineffective binding of Zn^{2+} to **L2**, **L4**, and **L6** might be the basis of nonfluorescent nature of Zn complexes of **L2**, **L4**, and **L6**. The keto form of **L6** is only slightly more stable than the enol-form, but the presence of the NO_2 group also might cause a weak binding with Zn^{2+}.

The conformation of free ligands **L1**, **L3**, **L5**, and **L7** (enol-forms, Figure 3) and their corresponding Zn^{2+} complexes are nearly the same, and Figure 4 shows the optimized structure of **L1** along with its frontier molecular orbitals (optimized structures of all other ligands and corresponding Zn complexes are given in the Supporting Information, Figures S45−S56). In **L1**, a strong hydrogen bond between the OH hydrogen and N (N−H distance is 1.72 Å) stabilizes the enol-form. The HOMO-1 is the π-orbital of the phenyl ring and the lone pair orbitals on N and S, while the HOMO is formed by the mixing of the π-orbital of the naphthyl ring and the lone pair orbital of S. LUMOs are the corresponding π^*-orbitals. The HOMO−LUMO energy gap is 4.25 eV (Figure 4a). The binding of **L1** to Zn^{2+} initially would lead to the formation of the complex **L1−OH−Zn**$^{2+}$ (Figure 4b) in which Zn^{2+} is coordinated to **L1** through the lone pairs on N and O. The binding of N with Zn^{2+} in **L1−OH−Zn**$^{2+}$ is very strong since the Zn−N distance is 1.94 Å, while the Zn−O distance is 2.11 Å. The strong Zn−N interaction leads to a charge transfer from N and the phenyl group to the metal center; therefore, the HOMO-1 and HOMO of **L1−OH−Zn**$^{2+}$ are formed by the mixing of π-

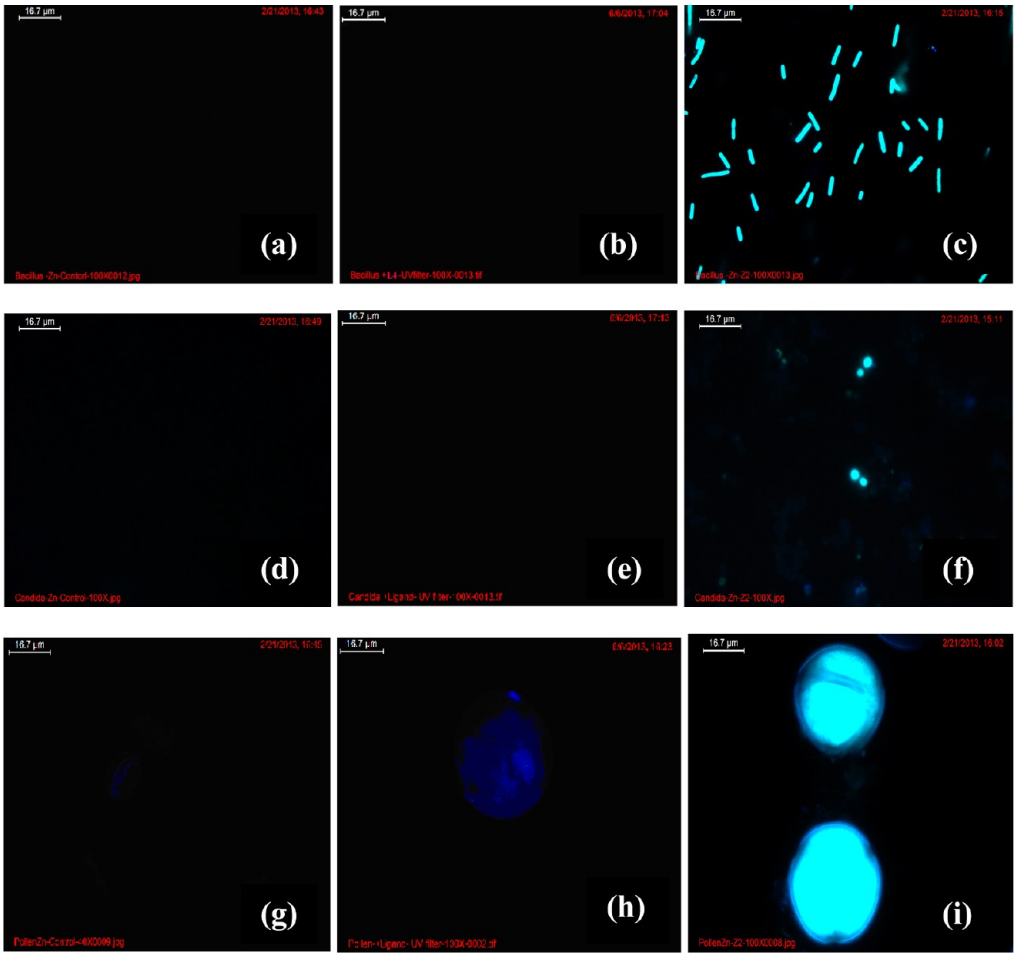

Figure 7. Fluorescence microscopic photographs of (a) *Bacillus thuringiensis* cells treated with Zn^{2+}, (b) *B. thuringiensis* cells treated with **L5**, (c) *B. thuringiensis* cells treated with Zn^{2+} followed by **L5**, (d) *Candida albicans* cells treated with Zn^{2+}, (e) *C. albicans* cells treated with **L5**, (f) *C. albicans* cells treated with Zn^{2+} followed by **L5**, (g) *Techoma stans* pollen grains treated with Zn^{2+}, (h) *T. stans* treated with **L5**, and (i) *T. stans* treated with Zn^{2+} followed by **L5** (scale bar 16.7 μM).

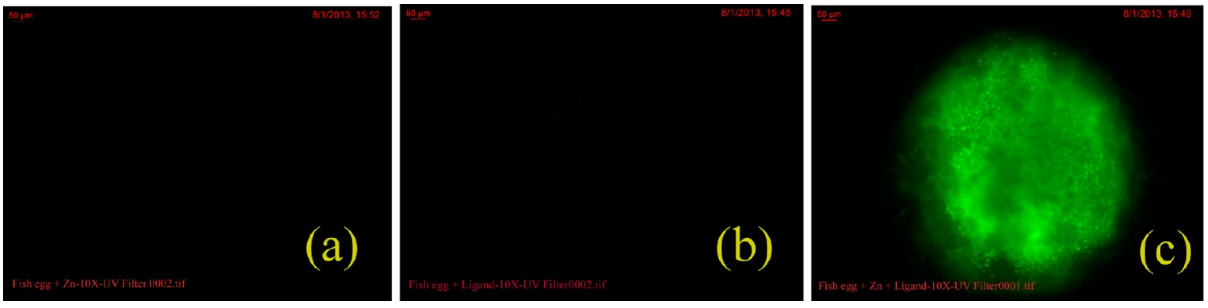

Figure 8. Fluorescence microscopic photograph of fish egg treated with (a) Zn^{2+}, (b) **L5**, and (c) Zn^{2+} followed by **L5** (scale bar 50 μM).

orbitals on the naphthyl rings, while the LUMOs are the π^*-orbitals of the phenyl moiety (Figure 5). The HOMO−LUMO energy gap in **L1−OH−Zn**$^{2+}$ is 0.99 Å. A red shift in the absorption spectra of **L1** after the addition of Zn^{2+} results from the lowering of the HOMO−LUMO energy gap in **L1−OH−Zn**$^{2+}$. It should be noted that the HOMO and LUMO of **L1** are in different planes, but the coordination of Zn^{2+}-linearized **L1** and therefore the HOMO and LUMO of **L1−OH−Zn**$^{2+}$ are in the same plane which might be the basic reason for the generation of fluorescence in **L1−OH−Zn**$^{2+}$ (orbital symmetries of HOMOs and LUMOs are the same). Addition of strong anions to **L1−OH−Zn**$^{2+}$ could easily remove H^+ from the OH, leading to the formation of **L1−Zn**$^{2+}$ (Figure 4b). In **L1−Zn**$^{2+}$ both the N lone pair and O^- are strongly interacting with Zn^{2+} since Zn−N and Zn−O distances are 2.01 and 1.93 Å, respectively. The HOMOs are formed by the mixing of π-orbitals of the phenyl ring and the lone pair orbitals on O and S, while LUMOs are the corresponding π^*-orbitals (Figure 6). The enhancement of fluorescence by the formation of **L1−Zn**$^{2+}$ might result from the electronic transition between the orbitals of same symmetry which are on the same moiety.

Biological Studies. To examine the efficacy of **L5** in imaging intracellular zinc, initially three different types of cells, viz., *Candida albicans*, *Bacillus thuringiensis*, and pollen grains,

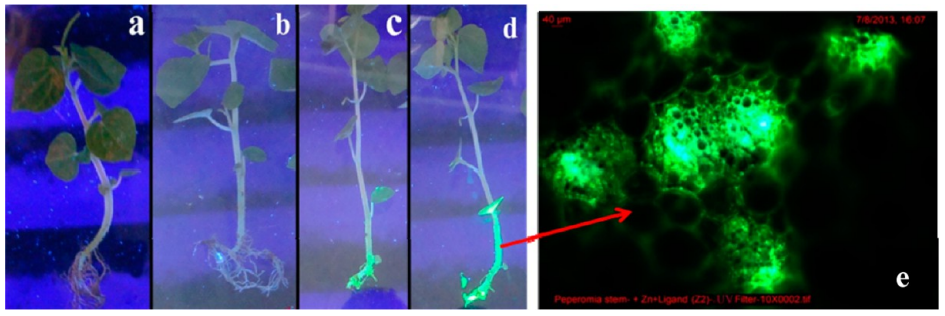

Figure 9. Fluorescence micrograph of whole plant treated with (a) Zn^{2+}, (b) probe **L5**, (c) Zn^{2+} for one hour followed by **L5** for 30 min, (d) Zn^{2+} for one hour followed by **L5** for one hour, and (e) transverse section of *Peperomia pellucida*, treated with Zn^{2+} for one hour followed by **L5** for one hour, fluorescing vascular bundle (observed under fluorescence microscope) (scale bar 40 μM).

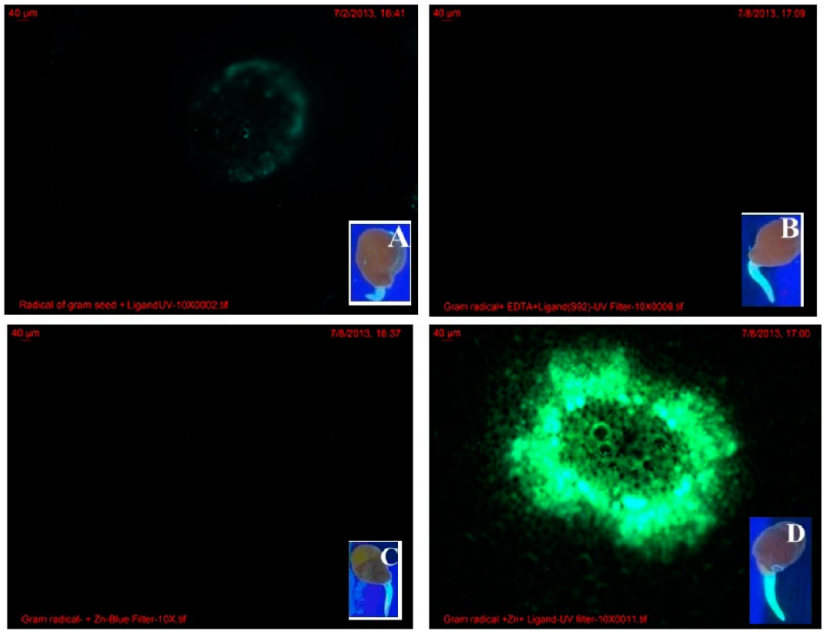

Figure 10. Transverse section of Gram radicals showing a vascular bundle after respective treatment of (A) **L5** for one hour, (B) EDTA for one hour followed by **L5** for another one hour, (C) Zn^{2+} for one hour, and (D) Zn^{2+} for one hour followed by **L5** for one hour (scale bar 40 μM).

were used. These cells were first incubated with Zn^{2+} followed by probe **L5**. The incubated cells were then mounted on a grease-free glass slide and observed under a Leica DM 1000 fluorescence microscope with a UV filter. A strong green fluorescence was observed which clearly indicated the cell permeability and intracellular zinc imaging potential of **L5** (Figure 7). As a control experiment following a reverse sequence of incubation, when *Candida albicans* cells were treated with **L5** followed by Zn^{2+}, similar bright green fluorescence was observed which indicated that Zn^{2+} imaging was not sequence dependent, confirming the high affinity of probe **L5** towards Zn^{2+} (Figure S57, Supporting Information). It is worth mentioning that probe **L5** did not experience any interference of cellular phosphates while imaging zinc in a cellular environment. Interestingly, pyrophosphate-overloaded *Candida albicans* cells also showed promising bright green fluorescence when treated with **L5** followed by Zn^{2+} (Figure S58, Supporting Information).

Further application of **L5** in detecting intracellular zinc in animal cells was established using eggs of *Puntius sarana sarana*. When zinc-treated eggs were incubated with **L5** and observed under a fluorescence microscope, a strong green emission confirmed successful imaging of zinc inside animal cells (Figure 8). No such emission from controls was observed.

MTT assay was performed to evaluate the toxic effect, if any, of **L5** on *Candida* cells.[74−77] The assay was performed in the presence of zinc salt and **L5**, and the results indicated that the cells treated with Zn^{2+} followed by **L5** in increasing concentrations (400 nM, 4 μM, and 3 mM) showed a slight decrease in viability which is directly proportional to their concentration. Therefore, **L5** does not have any strong detrimental effect on cell viability, and it permeates the cell membrane without causing any significant harm to the cells (Figure S59, Supporting Information).

With the success in in vitro imaging, we became interested in knowing the in vivo imaging potential of **L5**. Plant systems were used for studying in vivo zinc imaging using the **L5** molecular marker. At various intervals of time, the movement of **L5** and translocation of zinc through a stem of *Peperomia pellucida* were efficiently imaged (Figure 9). This imaging experiment supported the possibility of using **L5** in fluorescence imaging of zinc in living systems in real time. As in vivo imaging experiments using animal models are always expensive and associated with lengthy processes, one may

practically be guided by this approach in screening in vivo imaging potential of a probe, particularly its stability and real-time analysis possibility inside living systems, before being tested on animals.

As **L5** was found to be stable inside living systems and efficient enough in detecting/imaging zinc in different kinds of biological systems, our final aim was the utilization of **L5** in the detection and localization of zinc in cereal sprouts. As zinc is an important and essential micronutrient for both animals and plants,[78,79] zinc deficiency may lead to several disorders in biological processes. As the people of developing countries consume a large amount of cereal crops, the human zinc deficiency could partially be compensated by eating zinc-enriched cereal crops.[80] Zinc enrichment in these crops largely depends on soil-zinc concentration, and many areas of the world suffer from soil-zinc deficiency. Therefore, several strategies (such as genetic biofortification, agronomic biofortification, etc.) have been developed over the years to increase zinc enrichment in cereal crops.[79] Some techniques that are used for the detection and localization of zinc in cereal crops are inductively-coupled plasma-optical emission spectroscopy (ICP-OES),[80,81] energy-dispersive X-ray fluorescence (EDXRF),[82] etc. However, all these techniques are either expensive or require large amounts of samples. As zinc mobilization occurs from seed to sprout during seed germination, the detection and localization of sprout-zinc may provide an idea about crops' zinc enrichment. Therefore, we became interested in using fluorescence imaging techniques for the detection and localization of sprout-zinc with the help of **L5** as a zinc-specific green-emissive molecular marker. When zinc-treated gram seed sprouts were incubated with **L5** and observed under a fluorescence microscope, fluorescence imaging of sprout-zinc with bright green emission was observed (Figure 10D). Interestingly, **L5** was found to be efficient enough to detect a native zinc pool of seed sprout (Figure 10A). This was confirmed from the fact that no such imaging was observed when an EDTA-treated sprout was incubated with **L5** (Figure 10B, strong complexation between EDTA and zinc made zinc inaccessible to **L5**). Therefore, this method could be a potential and easy alternative in investigating the efficiency of various strategies used for zinc enrichment in cereal crops. To the best of our knowledge, such an analytical approach on zinc imaging of this kind has not been reported previously.

CONCLUSION

To conclude, systematic structure-fluorescence/interaction studies helped in developing a small chemical library of cysteamine-based cell-permeable molecular probes. Some of the probes of this family upon interaction with Zn^{2+} resulted in the generation of strong fluorescence signal. As the origin of fluorescence of probe–Zn^{2+} ensembles was mainly due to the ICT mechanism, and as the extent of chelation was largely dependent on the electronic properties of the binding site, the emission spectra were different for different probes. Detailed theoretical studies enabled us to understand some of the experimental findings. Due to its higher excitation/emission wavelengths, **L5** was chosen as a model compound for biological studies. **L5** was found to be potent for imaging zinc in biological systems, both in vitro and in vivo. Whereas in vitro studies were performed using four different kinds of cells, in vivo studies were carried out in plant systems. The imaging of translocation of zinc through the stem at different intervals of time indicated the possibility of using **L5** for real-time analysis. In addition, the present approach may help in knowing the in vivo imaging potential of a newly developed probe using a plant model before applying it to the expensive animal model. On the other hand, the approach of applying a probe in the detection and localization of zinc in gram seed sprouts through in vivo imaging could be quite useful in investigating the efficiency of various strategies used for zinc enrichment in cereal crops.

ASSOCIATED CONTENT

Supporting Information

Synthesis procedures and scan copies of ^{1}H NMR, ^{13}C NMR, and mass spectra. Additional spectral data on UV–Vis and fluorescence studies. This material is available free of charge via the Internet at http://pubs.acs.org.

AUTHOR INFORMATION

Corresponding Authors

*Tel.: +91-1905-237926. Fax: +91-1905-237924. E-mail: subrata@iitmandi.ac.in.

*E-mail: skmmicro@gmail.com.

Notes

The authors declare no competing financial interest.

ACKNOWLEDGMENTS

Financial support was received from the Department of Science and Technology, India (Grant No. SERB/F/2408/2012-13). SS, GD, and SK are grateful to IIT Mandi for their fellowship. We thankfully acknowledge the Director, IIT Mandi, for research facilities. The support of Advanced Materials Research Center (AMRC), IIT Mandi, for sophisticated instrument facility is thankfully acknowledged. We also gratefully acknowledge the support of USIC (Burdwan University) for the fluorescence microscope facility. We are thankful to the reviewers for their valuable comments.

DEDICATION

The paper is dedicated to Professor Christoph Schneider.

REFERENCES

(1) Nolan, E. M.; Lippard, S. J. *Acc. Chem. Res.* **2009**, *42*, 193–203.
(2) Yang, Y.; Zhao, Q.; Feng, W.; Li, F. *Chem. Rev.* **2013**, *113*, 192–270.
(3) Terai, T.; Nagano, T. *Pflug Arch- Eur. J. Phy.* **2013**, *465*, 347–359.
(4) Kikuchi, K.; Komatsu, K.; Nagano, T. *Curr. Opin. Chem. Biol.* **2004**, *8*, 182–191.
(5) Vallee, B. L. *Physiol. Rev.* **1959**, *39*, 443–490.
(6) Sun, F.; Zhang, G.; Zhang, D.; Xue, L.; Jiang, H. *Org. Lett.* **2011**, *13*, 6378–6381.
(7) Cuajungco, M. P.; Lees, G. J. *Neurobiol. Dis.* **1997**, *4*, 137–169.
(8) Choi, D. W.; Koh, J. Y. *Annu. Rev. Neurosci.* **1998**, *21*, 347–375.
(9) Maret, W.; Jacob, C.; Vallee, B. L.; Fischer, E. H. *Proc. Natl. Acad. Sci. U.S.A.* **1999**, *96*, 1936–1940.
(10) Zalewski, P. D.; Forbes, I. J.; Betts, W. H. *Biochem. J.* **1993**, *296*, 403–0.
(11) Falchuk, K. H. *Mol. Cell. Biochem.* **1998**, *188*, 41–48.
(12) Vallee, B. L.; Falchuk, K. H. *Physiol. Rev.* **1993**, *73*, 79–118.
(13) Kimura, E.; Koike, T. *Chem. Soc. Rev.* **1998**, *27*, 179–184.
(14) Lippard, S. J.; Berg, J. M. *Principles of Bioinorganic Chemistry*; University Science Books: Mill Valley, CA, 1994.
(15) Walkup, G. K.; Burdette, S. C.; Lippard, S. J.; Tsien, R. Y. *J. Am. Chem. Soc.* **2000**, *122*, 5644–5645.
(16) Sensi, S. L.; Ton-That, D.; Sullivan, P. G.; Jonas, E. A.; Gee, K. R.; Kaczmarek, L. K.; Weiss, J. H. *Proc. Natl. Acad. Sci. U.S.A.* **2003**, *100*, 6157–6162.

(17) Burdette, S. C.; Walkup, G. K.; Spingler, B.; Tsien, R. Y.; Lippard, S. J. *J. Am. Chem. Soc.* **2001**, *123*, 7831−7841.
(18) Zalewski, P. D.; Forbes, I. J.; Seamark, R. F.; Borlinghaus, R.; Betts, W. H.; Lincoln, S. F.; Ward, A. D. *Chem. Biol.* **1994**, *1*, 153−161.
(19) Lim, N. C.; Yao, L.; Freake, H. C.; Bruckner, C. *Bioorg. Med. Chem. Lett.* **2003**, *13*, 2251−2254.
(20) Hirano, T.; Kikuchi, K.; Urano, Y.; Higuchi, T.; Nagano, T. *Angew. Chem., Int. Ed. Engl.* **2000**, *39*, 1052−1054.
(21) Hirano, T.; Kikuchi, K.; Urano, Y.; Nagano, T. *J. Am. Chem. Soc.* **2002**, *124*, 6555−6562.
(22) Gee, K. R.; Zhou, Z.-L.; Qian, W.-J.; Kennedy, R. *J. Am. Chem. Soc.* **2002**, *124*, 776−778.
(23) Burdette, S. C.; Frederickson, C. J.; Bu, W.; Lippard, S. J. *J. Am. Chem. Soc.* **2003**, *125*, 1778−1787.
(24) Maruyama, S.; Kikuchi, K.; Hirano, T.; Urano, Y.; Nagano, T. *J. Am. Chem. Soc.* **2002**, *124*, 10650−10651.
(25) Qian, W.-J.; Gee, K. R.; Kennedy, R. T. *Anal. Chem.* **2003**, *75*, 3468−3475.
(26) Gee, K. R.; Zhou, Z. L.; Ton-That, D.; Sensi, S. L.; Weiss, J. H. *Cell Calcium* **2002**, *31*, 245−251.
(27) Sensi, S. L.; Ton-That, D.; Weiss, J. H.; Rothe, A.; Gee, K. R. *Cell Calcium* **2003**, *34*, 281−284.
(28) Nolan, E. M.; Jaworski, J.; Okamoto, K.-I.; Hayashi, Y.; Sheng, M.; Lippard, S. J. *J. Am. Chem. Soc.* **2005**, *127*, 16812−16823.
(29) Nolan, E. M.; Jaworski, J.; Racine, M. E.; Sheng, M.; Lippard, S. J. *Inorg. Chem.* **2006**, *45*, 9748−9757.
(30) Woodroofe, C. C.; Masalha, R.; Barnes, K. R.; Frederickson, C. J.; Lippard, S. J. *Chem. Biol.* **2004**, *11*, 1659−1666.
(31) Chang, C. J.; Nolan, E. M.; Jaworski, J.; Burdette, S. C.; Sheng, M.; Lippard, S. J. *Chem. Biol.* **2004**, *11*, 203−210.
(32) Lim, N. C.; Freake, H. C.; Bruckner, C. *Chem.−Eur. J.* **2005**, *11*, 38−49.
(33) Ueno, S.; Tsukamoto, M.; Hirano, T.; Kikuchi, K.; Yamada, M. K.; Nishiyama, M.; Nagano, T.; Matsuki, N.; Ikegaya, Y. *J. Cell. Biol.* **2002**, *158*, 215−220.
(34) Fang, X.; Li, H.; Zhao, G.; Fang, X.; Xu, J.; Yang, W. *Biosens. Bioelectron.* **2013**, *42*, 308−313.
(35) Lee, S.; Lee, J. H.; Pradhan, T.; Lim, C. S.; Cho, B. R.; Bhuniya, S.; Kim, S.; Kim, J. S. *Sens. Actuators, B* **2011**, *160*, 1489−1493.
(36) Ding, Y.; Xie, Y.; Li, X.; Hill, J. P.; Zhang, W.; Zhu, W. *Chem. Commun.* **2011**, *47*, 5431−5433.
(37) Xu, Z.; Liu, X.; Pan, J.; Spring, D. R. *Chem. Commun.* **2012**, *48*, 4764−4766.
(38) Liu, Z.; Zhang, C.; Chen, Y.; He, W.; Guo, Z. *Chem. Commun.* **2012**, *48*, 8365−8367.
(39) Kumar, M.; Kumar, N.; Bhalla, V. *Chem. Commun.* **2013**, *49*, 877−879.
(40) Kim, J. H.; Hwang, I. H.; Jang, S. P.; Kang, J.; Kim, S.; Noh, I.; Kim, Y.; Kim, C.; Harrison, R. G. *Dalton Trans.* **2013**, *42*, 5500−5507.
(41) Sarkar, S.; Khuda-Bukhsh, A. R.; Mukherjee, M.; Helliwell, M.; Chattopadhyay, P. *Inorg. Chem.* **2011**, *50*, 1213−1219.
(42) Iyoshi, S.; Taki, M.; Yamamoto, Y. *Org. Lett.* **2011**, *13*, 4558−4561.
(43) Chang, C. J.; Jaworski, J.; Nolan, E. M.; Sheng, M.; Lippard, S. J. *Proc. Natl. Acad. Sci. U.S.A.* **2004**, *101*, 1129−1134.
(44) Zhou, Y.; Li, Z.-X.; Zang, S.-Q.; Zhu, Y.-Y.; Zhang, H.-Y.; Hou, H.-W.; Mak, T. C. W. *Org. Lett.* **2012**, *14*, 1214−1217.
(45) Pisoni, R. L.; Park, G. Y.; Velilla, V. Q.; Thoene, J. G. *J. Biol. Chem.* **1995**, *270*, 1179−1184.
(46) Kim, M. J.; Kaur, K.; Singh, N.; Jang, D. O. *Tetrahedron* **2012**, *68*, 5429−5433.
(47) Wang, L.; Qin, W.; Tang, X.; Dou, W.; Liu, W. *J. Phys. Chem. A* **2011**, *115*, 1609−1616.
(48) Zhang, Y.; Guo, X.; Jia, L.; Xu, S.; Xu, Z.; Zheng, L.; Qian, X. *Dalton Trans.* **2012**, *41*, 11776−11782.
(49) Zhang, Y.; Guo, X.; Si, W.; Jia, L.; Qian, X. *Org. Lett.* **2008**, *10*, 473−476.
(50) Roy, P.; Dhara, K.; Manassero, M.; Ratha, J.; Banerjee, P. *Inorg. Chem.* **2007**, *46*, 6405−6412.
(51) Dayal, D.; Palanimuthu, D.; Shinde, S.; Somasundaram, K.; Samuelson, A. *J. Biol. Inorg. Chem.* **2011**, *16*, 621−632.
(52) Karak, D.; Das, S.; Lohar, S.; Banerjee, A.; Sahana, A.; Hauli, I.; Mukhopadhyay, S. K.; Safin, D. A.; Babashkina, M. G.; Bolte, M.; Garcia, Y.; Das, D. *Dalton Trans.* **2013**, *42*, 6708−6715.
(53) Zhou, Y.; Li, Z.-X.; Zang, S.-Q.; Zhu, Y.-Y.; Zhang, H.-Y.; Hou, H.-W.; Mak, T. C. W. *Org. Lett.* **2012**, *14*, 1214−1217.
(54) Tochtrop, G. P.; Sadhukhan, S.; Koner, R. R.; Ghosh, S. *Tetrahedron* **2009**, *65*, 10515−10534.
(55) Ghosh, S.; Tochtrop, G. P. *Tetrahedron Lett.* **2009**, *50*, 1723−1726.
(56) Brodin-Sartorius, A.; Tete, M.-J.; Niaudet, P.; Antignac, C.; Guest, G.; Ottolenghi, C.; Charbit, M.; Moyse, D.; Legendre, C.; Lesavre, P.; Cochat, P.; Servais, A. *Kidney Int.* **2012**, *81*, 179−189.
(57) Cherqui, S. *Kidney Int.* **2012**, *81*, 127−129.
(58) Chakrabarti, E.; Ghosh, S.; Sadhukhan, S.; Sayre, L.; Tochtrop, G. P.; Smith, J. D. *J. Med. Chem.* **2010**, *53*, 5302−5319.
(59) Brown, A. D. et al.; *PCT Int. Appl.* 2004, WO 2004108675 A1 20041216.
(60) Moss, R. D.; Hamilton, P. M. Sulfur-containing schiff's bases 1964. US 3147307 19640901.
(61) V. Alfimov, M.; V. Churakov, A.; V. Fedorov, Y.; A. Fedorova, O.; P. Gromov, S.; E. Hester, R.; A. K. Howard, J.; G. Kuz'mina, L.; K. Lednev, I.; N. Moore, J. *J. Chem. Soc., Perkin Trans. 2* **1997**, 2249−2256.
(62) Kubo, Y.; Kato, M.; Misawa, Y.; Tokita, S. *Tetrahedron Lett.* **2004**, *45*, 3769−3773.
(63) Bhalla, V.; Roopa; Kumar, M. *Dalton Trans.* **2013**, *42*, 975−980.
(64) Choi, J. Y.; Kim, D.; Yoon, J. *Dyes Pigm.* **2013**, *96*, 176−179.
(65) Caballero, A.; Martínez, R.; Lloveras, V.; Ratera, I.; Vidal-Gancedo, J.; Wurst, K.; Tárraga, A.; Molina, P.; Veciana, J. *J. Am. Chem. Soc.* **2005**, *127*, 15666−15667.
(66) Job, P. *Ann. Chim. Appl.* **1928**, *9*, 113−203.
(67) Foresman, J. B.; Head-Gordon, M.; Pople, J. A.; Frisch, M. J. *J. Phys. Chem.* **1992**, *96*, 135−149.
(68) Becke, A. D. *J. Chem. Phys.* **1993**, *98*, 5648−5652.
(69) Lee, C.; Yang, W.; Parr, R. G. *Phys. Rev. B* **1988**, *37*, 785−789.
(70) Frisch, M. J. et al.; *Gaussian 09*; Gaussian, Inc.: Wallingford, CT, 2010.
(71) Martínez, R. F.; Ávalos, M.; Babiano, R.; Cintas, P.; Jiménez, J. L.; Light, M. E.; Palacios, J. C. *Eur. J. Org. Chem.* **2011**, 3137−3145.
(72) Mennucci, B.; Cammi, R.; Tomasi, J. *J. Chem. Phys.* **1999**, *110*, 6858−6870.
(73) Cossi, M.; Scalmani, G.; Rega, N.; Barone, V. *J. Chem. Phys.* **2002**, *117*, 43−54.
(74) Meerloo, J. et al. Cell Sensitivity Assays: The MTT Assay. *Cancer Cell Culture: Methods and Protocols*, 2nd ed.; Methods in Molecular Biology; Springer: New York, 2011; DOI 10.1007/978-1-61779-080-5_20; vol. 731.
(75) Tim, M. *J. Immunol. Methods* **1983**, *65* (1−2), 55−63.
(76) Berridge, M. V.; Herst, P. M.; Tan, A. S. *Biotechnol. Annu. Rev.* **2005**, *11*, 127−152.
(77) Slater, T.F.; Sawyer, B.; Strauli, U. D. *Biochim. Biophys. Acta* **1963**, *77*, 383−393.
(78) Fard, S. R.; Khourgami, A.; Rafee, M.; Nasrollahi, H. *Ann. Biol. Res.* **2012**, *3*, 4166−4171.
(79) Cakmak, I. *Plant Soil* **2008**, *302*, 1−17.
(80) Ozturk, L.; Yazici, M. A.; Yucel, C.; Torun, A.; Cekic, C.; Bagci, A.; Ozkan, H.; Braun, H. −J.; Sayers, Z.; Cakmak, I. *Physiol. Plant.* **2008**, *128*, 144−152.
(81) Steponėnienė, L.; Tautkus, S.; Kazlauskas, R. *Chemija (Vilnius)* **2003**, *14*, 99−102.
(82) Paltridge, N. G.; Palmer, L. J.; Milham, P. J.; Guild, G. E.; Stangoulis, J. C. R. *Plant Soil* **2012**, *361*, 251−260.